Physica Medica 60 (2019) 111–119

Contents lists available at ScienceDirect

Physica Medica

journal homepage: www.elsevier.com/locate/ejmp

Original paper

Identifying optimal clinical scenarios for synchrotron microbeam radiation therapy: A treatment planning study

Lloyd M.L. Smyth[a,b,*], Liam R. Day[c], Katrina Woodford[d,e], Peter A.W. Rogers[a], Jeffrey C. Crosbie[c,d], Sashendra Senthi[d,e]

[a] Department of Obstetrics & Gynaecology, University of Melbourne, Royal Women's Hospital, Parkville, Victoria 3052, Australia
[b] Icon Cancer Centre, Richmond, Victoria 3121, Australia
[c] School of Science, RMIT University, Melbourne, Victoria 3001, Australia
[d] Alfred Health Radiation Oncology, Alfred Health, Melbourne, Victoria 3004, Australia
[e] Department of Surgery, Central Clinical School, Monash University, Melbourne, Victoria 3004, Australia

ARTICLE INFO

Keywords:
Microbeams
Synchrotron X-rays
Treatment planning

ABSTRACT

Purpose: Synchrotron Microbeam Radiation Therapy (MRT) is a pre-clinical modality characterised by spatial dose fractionation on a microscopic scale. Treatment planning studies using clinical datasets have not yet been conducted. Our aim was to investigate MRT dose-distributions in scenarios refractory to conventional treatment and to identify optimal settings for a future Phase I trial.

Methods: MRT plans were generated for seven scenarios where re-irradiation was performed clinically. A hybrid algorithm, combining Monte Carlo and convolution-based methods, was used for dose-calculation. The valley dose to organs at risk had to respect the single fraction tolerance doses achieved in the corresponding re-irradiation plans. The resultant peak dose and the peak-to-valley dose ratio (PVDR) at the tumour target volume were assessed.

Results: Peak doses greater than 80 Gy in a single fraction, and PVDRs greater than 10, could be achieved for plans with small ($< 35\,cm^3$) or shallow volumes, particularly recurrent glioblastoma, head and neck tumours, and select loco-regionally recurrent breast cancer sites. Treatment volume was a more important factor than treatment depth in determining the PVDR. The mean PVDR correlated strongly with the size of the target volume ($r_s = -0.70$, $p = 0.01$). The PVDRs achieved in these clinical scenarios are considerably lower than those reported in previous pre-clinical studies.

Conclusion: Our findings suggest that head and neck sites will be optimal scenarios for MRT.

1. Introduction

For many recurrent, metastatic or treatment-resistant cancers, dismal prognosis persists despite the use of modern radiation oncology techniques. Synchrotron microbeam radiation therapy (MRT) is a pre-clinical modality that could improve outcomes through physical parameters and phenomena that are a departure from current radiobiological paradigms [1,2]. MRT is delivered as an array of quasi-parallel micro-planar beams tens of microns wide and spaced by hundreds of microns which generates an alternating peak-valley dose-distribution in tissue [3,4]. In pre-clinical models, peak (in-beam) doses are reported to be in the order of 50 times greater than the corresponding valley doses [5,6]. Several characteristics of synchrotron radiation are essential to maintaining a high-resolution peak-valley dose-distribution in tissue [7]; 1) a keV x-ray energy to minimise the range of secondary electrons, 2) an ultra-high dose-rate (several hundred Gray per second) to mitigate the effects of physiological tissue motion, and 3) minimal beam divergence.

In animal models, normal tissue tolerates single fraction MRT doses up to several hundred Gray [4,5,8–10] while tumour control can be achieved despite only a fraction of the tumour receiving the peak dose [11,12]. These observations challenge a central dogma of conventional radiation oncology; a dose-response and therapeutic index that is dependent on highly conformal doses delivered to the entire target volume, while avoiding adjacent organs at risk. For MRT, the therapeutic effect is thought to rely on optimising the interplay between the peak and valley doses [2,7], making the peak-to-valley dose ratio (PVDR) one key metric for assessing the effectiveness of clinical plans.

* Corresponding author at: Level 7, Royal Women's Hospital, Corner Grattan Street and Flemington Road, Parkville, Victoria 3052, Australia.
E-mail addresses: lloyd.smyth@icon.team (L.M.L. Smyth), liam.day@rmit.edu.au (L.R. Day), k.woodford@alfred.org.au (K. Woodford), parogers@unimelb.edu.au (P.A.W. Rogers), jeffrey.crosbie@rmit.edu.au (J.C. Crosbie), s.senthi@alfred.org.au (S. Senthi).

https://doi.org/10.1016/j.ejmp.2019.03.019
Received 3 December 2018; Received in revised form 20 February 2019; Accepted 19 March 2019
Available online 30 March 2019

Previous studies showing the possible PVDRs and peak doses achievable by MRT use simple, homogenous phantoms [7,13–17]. A smaller number of studies use more complex inhomogeneous phantoms of the human lung [18], human head [19–21] or rat spinal cord [5]. Importantly, many of these studies used field sizes suitable for either pre-clinical rodent irradiations or for small human tumours. Such results are generally not applicable to the re-irradiation setting in humans, particularly given the influence of field size on the PVDR [3].

Although cranial malignancies have been proposed as an ideal future target for MRT [1,2], no studies have demonstrated MRT dosimetry in different clinical contexts. The purpose of this treatment planning study is to identify optimal scenarios for MRT from a range of intracranial and extra-cranial targets. We limited our planning study to cases that could be justified for a future Phase I trial. These were cases of local or loco-regional recurrence(s) where re-irradiation was the only viable treatment option. Specifically, we aim to inform clinicians about the PVDRs achievable, the peak doses reasonably deliverable and clinical features that may be a contraindication for MRT. We hypothesise that the depth and volume of tumours will correlate with PVDR. To our knowledge, this is the first MRT treatment planning study to use clinical datasets.

2. Materials and methods

2.1. Clinical datasets

Seven clinical computed tomography (CT) datasets and corresponding external beam radiation therapy plans were supplied by Alfred Health Radiation Oncology following approval by the institutional Human Ethics Review Committee. Datasets were de-identified, anonymised and imported into a research version of the Eclipse™ (Varian Medical Systems, Palo Alto, CA) treatment planning system (TPS). We performed MRT planning using datasets for intra-cranial, head and neck, chest and spine sites. Details for the datasets, including demographic and clinical planning data, are summarised in Table 1. Patients included in this planning study had all developed predominantly local, symptomatic recurrence following radical radiotherapy treatment and were treated with re-irradiation using conventional fractionated treatment having exhausted systemic treatment options. In each case there were organ at risk (OAR) constraints limiting the total dose that could be delivered.

2.2. Treatment planning system characteristics

A hybrid MRT dose-calculation algorithm, previously described by Donzelli et al. [22], was implemented in the Eclipse™ TPS environment. In short, the hybrid algorithm calculates the dose delivered due to photon and electron mediated energy transport separately; Monte Carlo simulations calculate photon transport while secondary electron transport is calculated with a convolution-based algorithm. The resultant accuracy of the hybrid algorithm is comparable to pure Monte Carlo approaches but with substantially shorter, and clinically feasible, calculation times [22].

The algorithm was adapted to model the parameters of the Imaging and Medical Beamline (IMBL) at the Australian Synchrotron [3]. Additionally, the linear polarisation of the synchrotron x-ray beam was accounted for. MRT at the IMBL is delivered using an array of vertically orientated microbeams 50 μm wide with a centre-to-centre spacing of 400 μm. The microbeam energy spectrum is between 50 and 200 keV (mean energy of 94 keV) and the in-beam dose rate is approximately 300 Gy/s [3].The TPS limits the field width and length to 30 mm and 140 mm, respectively, and uses a fixed horizontal beamline which reflects the physical limitations of the IMBL. The TPS generates separate, corresponding plans for the peak and valley doses.

Table 1
Summary of clinical plans used for MRT planning.

Patient ID	Gender	Age at re-irradiation (Years)	Diagnosis	Primary irradiation dose (Gy)/Number of fractions	Site(s) of recurrence	Re-irradiation dose (Gy)/ Number of fractions	PTV Volume (cm^3)	Depth at centre of PTV (cm)	Re-irradiation technique
GBM1	F	52	Glioblastoma	60/30	Left temporal lobe	30/5	11.1	4.9	3 non-coplanar DCAs
GBM2	M	58	Glioblastoma	60/30	Right lateral ventricle	30/5	31.3	4.9	4 non-coplanar DCAs
HN1	M	70	Sino-nasal undifferentiated carcinoma	66/33	Left cavernous sinus	50/20	13.2	6.3	3 DCAs + 4 IMRT fields at 3 non-coplanar couch angles
HN2	F	64	Adenoid cystic carcinoma of the submandibular gland	60/30	Right base of skull	50/20	20.2	5.4	4 non-coplanar DCAs
Chest1	F	41	Multifocal invasive ductal carcinoma	50.4/28	Right IMC	50.4/28	223.2	3.0	5 static fields
					Right Neck	45/28	44.1	2.5	
					Right SCF/ICF		55.3	2.5	
Chest2	F	45	Infiltrating ductal carcinoma	50.4/28	Right IMC	50.4/28	84.1	2.4	5 IMRT fields
					Left IMC		77.0	2.3	
					Right ICF		35.4	2.8	
					Right Axilla		49.0	3.4	
					Right SCF		30.1	2.4	
Sac1	F	42	Schwannoma	Surgery	Sacrum	54/30	237.2	4.0	5 IMRT fields

PTV; planning target volume, DCA; dynamical conformal arc, IMRT; intensity modulated radiation therapy, SCF; supra-clavicular fossa, ICF; infra-clavicular fossa, IMC; internal mammary chain.

Table 2
Single fraction tolerance doses for organs at risk.

Plan	Number of Fractions	Organ at risk	Endpoint	α/β ratio	Fractionated dose (Gy)	Single Fraction equivalent dose (Gy)
GBM1	5	Brainstem	Cranial Neuropathy [26]	2.1 [26]	D_{max} = 8.8	D_{max} = 4.9
		Optic apparatus	Optic Neuropathy [27]	1.6 [27]	D_{max} = 1.9	D_{max} = 1.3
GBM2	5	Brainstem	Cranial Neuropathy	2.1	D_{max} = 24.6	D_{max} = 12.1
		Optic apparatus	Optic Neuropathy	1.6	D_{max} = 5.9	D_{max} = 3.3
HN1	20	Brainstem	Cranial Neuropathy	2.1	D_{max} = 20.7	D_{max} = 7.1
		Optic apparatus	Optic Neuropathy	1.6	D_{max} = 29.2	D_{max} = 8.7
HN2	20	Brainstem	Cranial Neuropathy	2.1	D_{max} = 30	D_{max} = 9.4
		Optic apparatus	Optic Neuropathy	1.6	D_{max} = 30	D_{max} = 8.9
Chest1	28	Spinal cord	Myelopathy [28]	0.87 [28]	D_{max} = 45	D_{max} = 10.1
		Lungs	Pneumonitis [29]	4 [29]	V20 Gy = 27.1%	V7.9 Gy = 27.1%
		Heart	Pericarditis [30]	2.5 [30]	D_{mean} = 35	D_{mean} = 10.3
Chest2	28	Spinal cord	Myelopathy	0.87	D_{max} = 45	D_{max} = 10.1
		Lungs	Pneumonitis	4	V20 Gy = 20.0%	V7.9 Gy < 20.0%
		Heart	Pericarditis [30]	2.5 [30]	D_{mean} = 35	D_{mean} = 10.3
Sac1	30	Spinal nerve roots	Neurological toxicity [31]	3 [31]	D_{max} = 56.6	D_{max} = 15.2
		Rectum	RTOG Grade ≥ 2 late toxicity [32]	3 [32]	D_{max} = 54.8	D_{max} = 14.8

Table 3
Dose-distributions achieved in MRT plans.

Patient ID/PTV	Valley dose for OARs	Mean PVDR for PTV	Mean Peak dose to PTV (Gy)	Median Peak dose (IQR) to PTV (Gy)
GBM1	Brainstem: D_{max} = 3.1 Gy Optic apparatus: D_{max} = 1.3 Gy Brain: V12 Gy = 0.1 cm^3	16.0	96.7	95.8 (87.1–105.3)
GBM2	Brainstem D_{max} = 5.5 Gy Optic apparatus: D_{max} = 2.5 Gy Brain: V12 Gy = 4.9 cm^3	10.2	87.6	86.8 (77.9–96.0)
HN1	Brainstem D_{max} = 4.2 Gy Optic apparatus D_{max} = 8.2 Gy Brain: V12 Gy = 4.9 cm^3	11.7	102.9	101.6 (91.0–112.6)
HN2	Brainstem D_{max} = 6.0 Gy Optic apparatus D_{max} = 8.9 Gy Brain: V12 Gy = 0.3 cm^3	9.4	81.2	75.2 (64.3–92.9)
Chest1	Spinal Canal D_{max} = 10.1 Gy			
R IMC	Lungs V7.9 Gy = 0.1%	8.7	62.4	57.6 (47.2–76.8)
R Neck	Heart D_{mean} = 1.8	11.1	67.0	65.1 (55.1–78.2)
R SCF/ICF		9.0	65.6	63.7 (56.7–71.9)
Total PTV		9.1	63.6	60.0 (49.6–76.1)
Chest2	Spinal Canal D_{max} = 10.0 Gy			
R IMC	Lungs V7.9 Gy = 7.9%	9.5	100.0	101.2 (77.8–119.4)
L IMC	Heart D_{mean} = 3.1	11.1	124.4	105.6 (85.2–199.6)
R IC		10.6	103.3	121.5 (102.1–143.0)
R Ax		11.4	103.0	98.1 (84.3–120.1)
R SCF		13.1	131.3	128.9 (113.8–149.5)
Total PTV		10.8	108.3	108.3 (86.9–125.4)
Sac1	Spinal nerve roots D_{max} = 13.5 Rectum: D_{max} = 14.8 Gy	7.5	47.7	45.7 (37.4–55.5)

IQR; Inter-quartile range, SCF; supra-clavicular fossa, ICF; infra-clavicular fossa, IMC; internal mammary chain.

2.3. Planning method and evaluation

The OAR constraints used for re-irradiation were used to generate acceptable MRT valley plans. Once an acceptable MRT valley plan was achieved, a corresponding MRT peak plan was generated to determine the peak doses that could be delivered throughout the target volumes. Dose-volume histograms and dose statistics from the Eclipse™ TPS were used to evaluate and compare the MRT and clinical treatment plans. A plan showing the PVDR was derived from the peak and valley plans for each dataset. PVDR depth profiles were generated based on a line parallel to the field direction and passing through the geometric centre of the target volume.

Because MRT might be delivered as a single fraction treatment [1,23], the tolerance doses for OARs achieved in the fractionated clinical plans were scaled to a single fraction equivalent. For organs that were not dose-limiting in the clinical plans, tolerance doses were scaled from QUANTEC recommendations. Scaling was based on the linear quadratic (LQ) model, as described previously [24], with α/β ratios sourced predominantly from QUANTEC studies. This is summarised in Table 2. Skin doses, which were not considered in the clinical plans but are relevant to MRT due to the use of a keV beam energy, were restricted to V26 Gy < 0.035 cm^3 and V23 Gy < 10 cm^3 [25]. The lens', oesophagus and trachea were not considered as OARs as they were not in close enough proximity to the target volumes to be considered relevant. The limitations of applying the LQ model to MRT, which uses high and heterogenous doses, will be discussed later.

A uni-directional field approach, required to preserve the peak-valley geometry optimal for normal tissue sparing [4], was used for all plans. Field directions for individual plans were chosen based on a balance between avoiding critical OARs and minimising the target depth relative to the field direction. Where the size of a target exceeded the field width or height restrictions at the IMBL, a series of fields were stitched together to achieve coverage. For the head and neck sites, plans assumed a supine position and direct lateral fields. For the remaining sites, plans assumed a seated position, with couch rotations used to change the field entrance angle.

2.4. Statistics

Spearman's rank correlation (r_s) was used to analyse the relationship between target volume characteristics and PVDR. Statistical

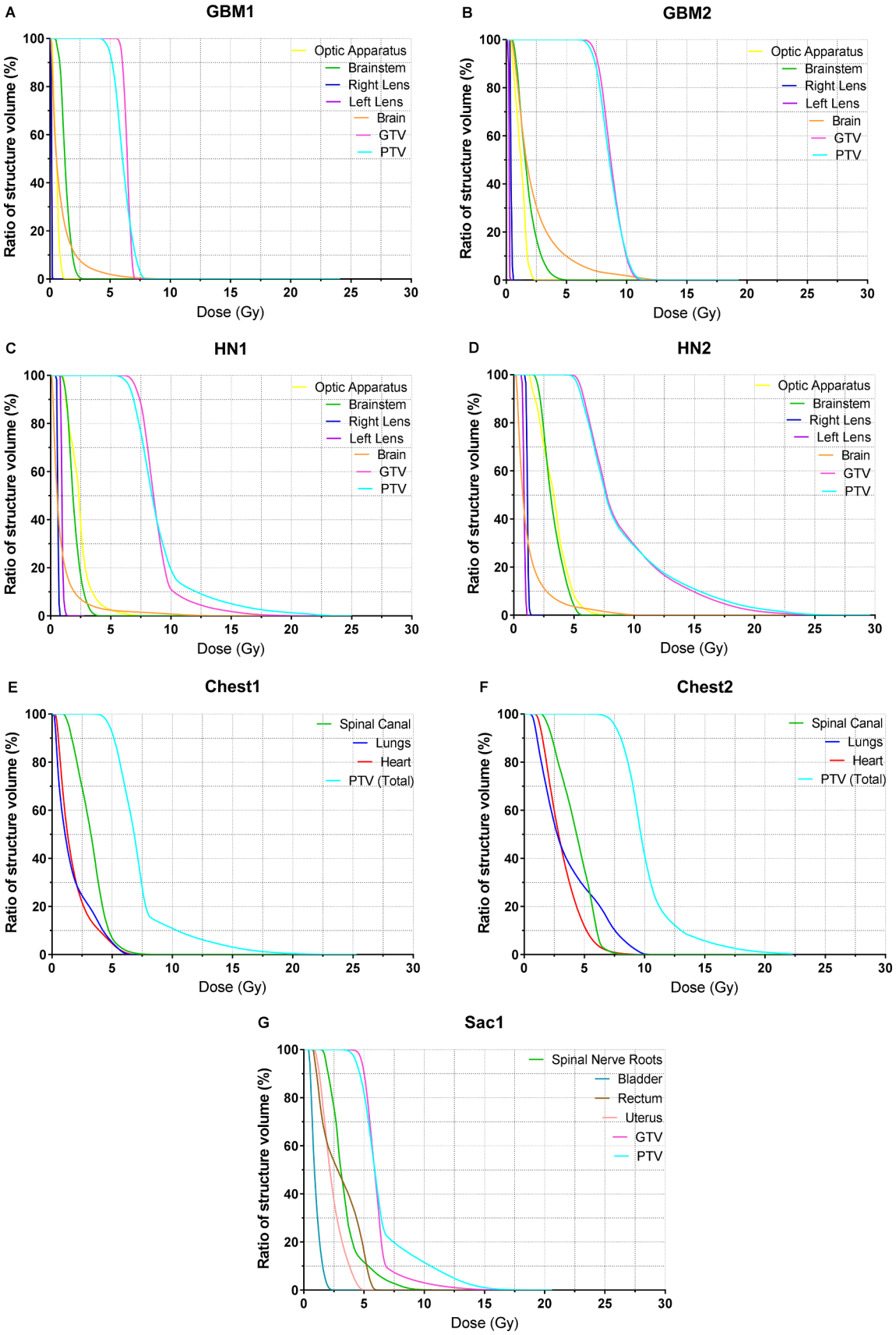

Fig. 1. Dose-volume histograms for single fraction MRT valley dose plans. The optic apparatus and brain were the most dose-limiting OARs for the glioblastoma (Panel A and B) and the head and neck (Panel C and D) recurrences. The spinal canal and rectum were the dose-limiting OARs for the loco-regionally recurrent breast cancer (Panel E and F) and sacral schwannoma (Panel G) plans, respectively.

analyses were performed using GraphPad Prism version 7.0 (GraphPad Software Inc, San Diego, California, USA), 95% confidence intervals are reported in square brackets and $p < 0.05$ was considered to be statistically significant.

3. Results

3.1. Valley dose to organs at risk

Table 3 summarises the dose-distributions achieved in the plans. Single fraction valley doses for each plan met the dose constraints achieved clinically and are displayed in dose-volume histograms (Fig. 1). Dose-volume histograms for the fractionated clinical plans are presented in Supplementary Fig. 1. For the recurrent glioblastoma and head and neck cases, the optic apparatus and the brain were the dose-limiting organs for MRT. Maximum valley doses to the brainstem were equal to or less than 6.0 Gy and clearly within tolerance. Very small volumes of the brain, limited to regions bordering the skull, received high doses, up to a maximum point dose of 24.1 Gy. However, the volume of brain receiving 12 Gy was less than 5 cm^3 in all cases [33]. Given its proximity to the bony spinal canal, the spinal cord was the most dose-limiting organ for the recurrent breast cancer plans. For the sacral schwannoma plan, the rectum was the dose-limiting normal tissue structure. The highest V26 Gy and V23 Gy values for the skin recorded across all the plans were 0.003 and 0.02 cm^3, respectively, both for a recurrent glioblastoma plan (GBM1). The maximum point dose to bone ranged from 20.5 for the sacral schwannoma (Sac1) to 46.7 Gy for the recurrent left cavernous sinus tumour (HN1).

3.2. Peak dose to target volumes

For acceptable doses to the OARs, the mean, single fraction peak doses ranged from 47.7 Gy for the sacral schwannoma (Sac1) to 131.3 Gy for the right supra-clavicular breast cancer recurrence (Chest2). The highest mean peak doses were achieved for plans with either small or superficial volumes. One of the recurrent breast cancer plans (Chest2) achieved mean peak doses greater than 100 Gy for all target volumes. The glioblastoma and head and neck plans still achieved mean peak doses of 80–100 Gy despite having the greatest treatment depths of all plans. The interquartile range for peak doses was largest for PTVs encompassing high or low-density regions, with bony regions responsible for very high maximum peak doses. The recurrent glioblastoma plans showed the least variation in peak dose across their respective PTVs, reflecting their location at depth within the brain and distance away from relatively low or high-density structures.

3.3. Peak to valley dose ratio

Mean PVDRs for the PTVs of each scenario ranged from 7.5 for the recurrent sacral schwannoma (Sac1) to 16.0 for a recurrent glioblastoma plan (GBM1). Even at depths greater than 5 to 6 cm, glioblastoma and head and neck plans could achieve PVDRs greater than 10. The mean PVDR correlated strongly with the size (i.e. volume) of the PTV ($r_s = -0.70$ [-0.90, -0.22], $n = 13$, $p = 0.01$) but no significant correlation was found between mean PVDR and central PTV depth (Fig. 2). There was a moderate, but not significant, negative correlation between mean PVDR and total field size ($r_s = -0.61$, $n = 7$, $p = 0.17$).

Fig. 3 illustrates the change in PVDR as a function of depth and tissue density. In soft tissue, PVDR was at a maximum at the field entrance and decreased sharply within the first 2 cm depth in tissue. The rate of decrease in PVDR reduced with depth, with PVDR approaching a plateau for most plans. The PVDR increased again very slightly as the field exited the body due to the loss of backscatter [13]. PVDR decreased sharply when moving from regions of soft tissue to bone and increased again sharply when moving back into soft tissue (Fig. 3A–G). This is explained by the increase in scattered irradiation in bone, which sharply increases the valley dose, thereby lowering the PVDR locally in that region [21]. The PVDR increases again distally to bone due to the relative loss of backscatter. Smaller target volumes, with smaller corresponding field sizes, had the highest entrance PVDR values and the highest PVDR plateaus. The PVDR approached zero in air gaps or cavities (Fig. 3A and D) due to a lack of dose deposition in these regions.

4. Discussion

The purpose of this treatment planning study was to inform clinicians about the dose-distributions possible with MRT, and in doing so, to identify optimal scenarios for its clinical testing. For an acceptable valley dose to OARs, shallow PTVs, or those with a volume less than 35 cm^3, achieved the highest PVDRs and peak doses. These scenarios included intra-cranial tumours, head and neck tumours, and select recurrent breast cancer sites. Treatment volume was a more critical factor than treatment depth in determining the PVDRs.

The PVDRs presented in our study are considerably lower than those reported in pre-clinical rodent studies, which are typically between 20 and 50 [5,6,34–36]. This observation is important given the centrality of peak-valley dosimetry to the novel radiobiology of MRT. Furthermore, previous studies presenting MRT dose-distributions typically use field sizes that would be too small to cover the target volumes selected in our study [3,19,21]. Consequently, clinically achievable PVDRs, in scenarios with a justification for a Phase I test, have previously been overestimated. For instance, Martinez-Rovira et al. [19] assume a field size of 2 cm^2 for a hypothetical intra-cranial tumour, yielding a substantially higher PVDR ($\sim$21) and lower valley doses compared to the intra-cranial tumour recurrences presented in our study.

Although small tumours are the most dosimetrically favourable for MRT, Phase I testing will not be justifiable in scenarios where combinations of surgery and stereotactic radiotherapy are routinely used [37–39]. However, a trial of MRT could be justified in settings where a standard, second line therapy for local recurrence has not been established and especially for patients with repeated local recurrences and poor prognosis. Datasets used in our study were selected from patients who had been offered potentially toxic re-irradiation in the clinic, in the context of no further surgical or systemic treatment options.

Glioblastoma Multiforme (GBM) is an example of an insidious disease which continues to have a dismal survival rate and limited therapeutic options for local recurrences despite significant research investment [40–42]. In our study, both GBM plans demonstrated features that might be favourable for MRT; relatively high PVDRs and mean peak doses to the PTV as well as a relatively low variation in peak dose across the target. Given the high incidence of GBM compared to other primary brain tumours, it should be possible to recruit a sub-set of patients with a treatment volume favourable for MRT.

Loco-regionally recurrent breast cancer is another clinical scenario where a trial of MRT could be justified, and in our study, showed potential for high peak doses to the target volume. The relatively shallow depth of the lymph nodes targeted in these plans favours the keV energy of MRT, with maximum peak doses and PVDRs occurring close to the skin surface. The difference in dose-distribution between the two recurrent breast cancer scenarios presented in our study can be explained by differences in the proximity of their respective PTVs to the dose-limiting spinal cord. The proximity of target volumes to the spinal canal could be a contraindication for MRT given the local increase in valley dose in bone which would increase the risk of spinal cord toxicity. To mitigate this risk, an angled, rather than direct anterior field approach, could be taken to completely avoid the MRT field exiting through or close to the spinal canal.

Given the dose-distributions observed in the loco-regionally recurrent breast cancer plans, superficially recurrent cancers or metastatic cutaneous lesions would also be dosimetrically favourable targets for MRT. Breast tumours which metastasize to the skin [43] and in-

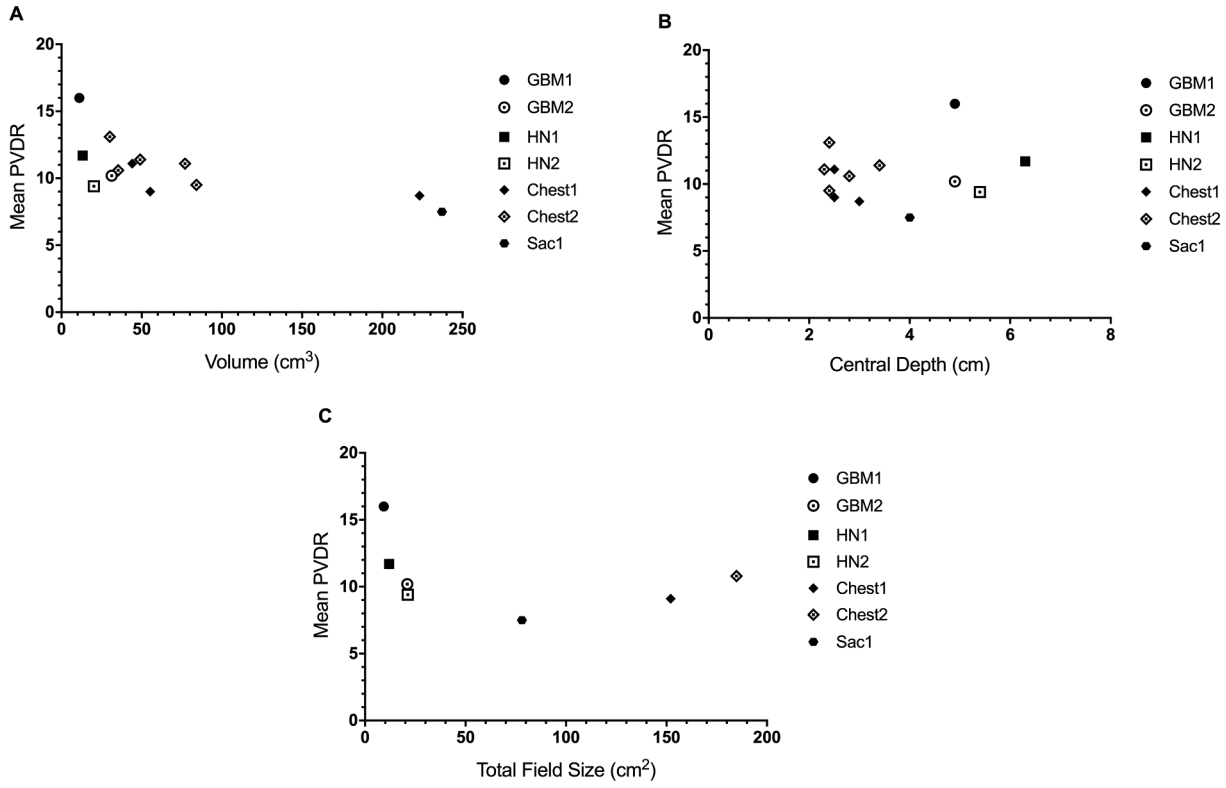

Fig. 2. Correlation plots of mean PVDR versus target size (Panel A), central target depth (Panel B) and total field size (Panel C). While the size of the PTV correlated strongly and negatively with PVDR ($r_s = -0.70$ [−0.90, −0.22], n = 13, p = 0.01), central PTV depth did not ($r_s = 0.007$ [−0.56, 0.57], n = 13, p = 0.98). Total field size showed a moderate, but non-significant, negative correlation with mean PVDR ($r_s = -0.61$, n = 7, p = 0.17). The minimum central PTV depth for the targets selected for MRT planning was 2.3 cm. The locoregionally recurrent breast cancer plans had multiple target volumes which were considered individually when evaluating target volume and depth but considered as a total PTV when evaluating total field size. Correlation was analysed using Spearman's rank correlation with $p < 0.05$ considered statistically significant.

transit cutaneous or sub-cutaneous melanoma recurrences [44] can be unresponsive to standard local and systemic therapies and remain a therapeutic challenge [45,46]. These scenarios would be good candidates for MRT and future dosimetric investigation is warranted. Recurrent melanoma confined to the limbs would be a particularly attractive target for a Phase I test of MRT, given the lack of closely situated vital organs.

Pragmatically speaking, the treatment of recurrent intra-cranial or head and neck lesions would currently be more feasible than breast cancer recurrences to the chest wall and regional lymph nodes. Firstly, patient-positioning solutions to overcome the limitations of the fixed horizontal beamline are more readily available for head and neck targets. A medical treatment chair has been implemented at the European Synchrotron Research Facility [47] and provides sufficient accuracy for stereotactic intra-cranial irradiations. This would be a feasible positioning solution for treatments of the head or neck at the IMBL. Positioning for extra-cranial treatment sites would be more difficult, however, a robotic patient positioning couch recently installed at the IMBL might be suitable for clinical purposes following further testing and development. Secondly, the accuracy of the hybrid algorithm in lung tissue remains a point of contention due to the complex pulmonary microstructure and the presence of air. This may preclude its use for thoracic treatment fields.

A potential disadvantage of treating intra-cranial tumours with MRT is the need for fields to traverse the skull prior reaching the target volume. Martinez-Rovira et al. [19] estimate that a maximum peak dose of 75–90 Gy would be deliverable to an intra-cranial tumour at a depth of 4.5–5.5 cm, if desiring to restrict the probability of long-term bone-related complications to less than 5% in 5 years [48]. The higher atomic number of bone is associated with an increased probability of Compton-scattered photons being absorbed in the valley region via the photo-electric effect, leading to a sharp increase in valley dose in the skull [21]. We chose to accept higher maximum valley doses to bone given that: 1) osteoradionecrosis is a late-effect of radiation and that for a Phase I test of MRT, acute toxicity would be the most relevant outcome for patients with an otherwise short life-expectancy (< 6 months), 2) bone is highly resistant to radiation, with single fraction doses of at least 50 Gy routinely used in the extracorporeal irradiation of malignant bone tumours [49,50], and, 3) if patients survive long enough to experience long-term osteoradionecrosis of the skull, cranioplasty is a common and well-established neurosurgical procedure to preserve cosmesis and brain protection [51].

A key assumption in our study, and of previous MRT dosimetry investigations [19], is that the MRT valley dose is the best parameter for the evaluation of normal tissue complication probability. A recently published *in vivo* study investigating the equivalence of MRT and conventional broad-beam radiation therapy in a murine model showed that median toxic valley doses were lower than the median toxic conventional radiation therapy dose by a factor of 1.6 to 1.8 [52]. This finding suggests that peak doses cannot be ignored in the context of MRT toxicity and that caution is required when assuming the equivalence of MRT valley dose with broad-beam dose. Further *in vivo* work is required to determine more precise and toxicity-specific scaling factors that would bring MRT valley doses to within OAR tolerance.

Further to this, we have used the LQ model to scale total fractionated OAR doses to a single fraction equivalent. While the applicability of the LQ model at high doses per fraction is controversial [53], there is robust data to suggest that the model is valid up to 10 Gy per fraction and sufficient data to justify its use in the design of clinical trials using 15–18 Gy per fraction [54–56]. The majority of the single fraction tolerance doses we utilized as dose constraints for the valley plans were less than 10 Gy. Additionally, our tolerance doses were at least as conservative as the single fraction tolerance doses recommended by

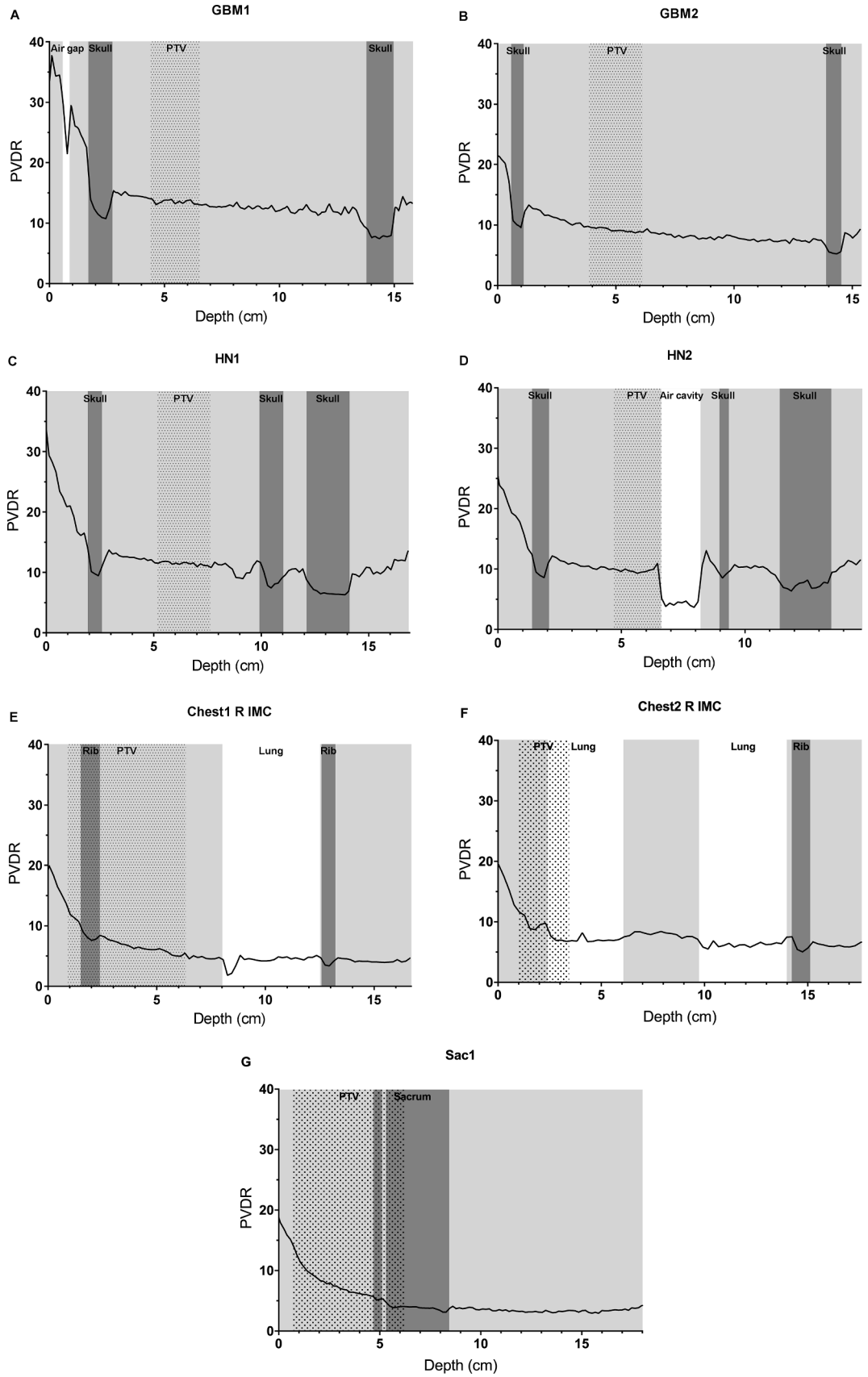

Fig. 3. PVDR depth profiles for individual target volumes within each patient plan. Glioblastoma (Panel A and B), head and neck (Panel C and D) and sacral schwannoma (Panel M) plans had a single PTV, while the locoregionally recurrent breast cancer plans (Panel E to L) had multiple PTVs. Regions of relatively high electron density, such as bone, are shaded in dark grey, while regions of relatively low density, such as lung, are white. PVDR increased sharply in regions of bone and approached zero in air (Panel A and D). In most cases, the PVDR increased marginally and gradually as the field passed through lung tissue, with sharper changes evident at tissue interfaces.

QUANTEC [57] or used in recent radiosurgery trials [25,58].

Importantly, all dose-calculations performed in this treatment planning study are specific to the photon spectrum of the IMBL which has a mean energy of 94 keV. The Eclipse™ TPS allows for the input of alternative spectra. The x-ray spectrum at the ID-17 beamline at the European Synchrotron Radiation Facility (ESRF) is similar but slightly more energetic than the IMBL with a mean photon energy of 105 keV [59]. The variation of PVDR with spectrum energy has been well documented [60–63]. Livingstone et al. [60] showed small increases in PVDR with increasing energy spectra up to a mean of 124 keV. Other studies have shown optimal mean x-ray energies for maximal PVDR as high as 175 keV to 300 keV [61,62]. For a given microbeam collimator geometry and field size, the PVDR is expected to be marginally higher at the ESRF compared to the IMBL. Shifts in mean energy spectra associated with kilovoltage x-ray beams in the range of 10 keV do not drastically affect PVDR. Rather, collimator geometry, field size and depth in material affects PVDR more profoundly than small changes in mean energy [60]. However, PVDR degradation is observed at mean energies higher than 300 keV due to the substantially increased range of secondary electrons travelling into the valley regions [62]. Mean photon energies up to 124 keV are technically feasible at the IMBL through increased filtration of the synchrotron light source. However, in order to maintain higher dose-rates suitable for the clinical delivery of MRT, a 95 keV mean energy is considered to be an appropriate compromise [60].

Finally, dosimetric validation of the TPS based on measurements of the peak and valley doses at various depths in three-dimensional heterogenous media is the next essential step towards use of this TPS in future veterinary or clinical studies. Previous studies have reported microbeam dosimetry data using a synthetic micro-diamond detector in a liquid water tank on the IMBL [3,64]. Experimental validation of the TPS is beyond the scope of this study but will be the focus of future work.

5. Conclusions

Based on our data, recurrent head and neck cancers could be an optimal scenario for a future Phase I trial of MRT, especially when also considering patient positioning solutions and the physical limitations of the IMBL. Selected patients with intra-cranial disease could also be suitable, given that high skull doses are deemed clinically acceptable. Superficially recurrent or cutaneous metastatic lesions should be investigated further. While the PVDRs presented in this study are relatively low, peak doses that are a factor of ten larger that the tissue tolerance dose are still possible. This could profoundly improve the therapeutic effect of radiation therapy and is worth exploring in clinical scenarios where alternative options have been exhausted or where standard therapeutic strategies have not been established.

6. Declarations of interest

None.

Funding

Funding sources were not involved in study design, the collection, analysis and interpretation of data, in the writing of the report, or in the decision to submit the article for publication.

Acknowledgements

L.S. is supported by a Research Training Program scholarship from the Australian Government Department of Education and Training. This project was supported by a grant from the Australian National Health and Medical Research Council [Project Grant 1061772]. The authors thank Frank Gagliardi and Vanessa Panetierri at Alfred Health Radiation Oncology for anonymising and exporting the clinical radiation therapy datasets for MRT planning use.

Appendix A. Supplementary data

Supplementary data to this article can be found online at https://doi.org/10.1016/j.ejmp.2019.03.019.

References

[1] Grotzer MA, Schultke E, Brauer-Krisch E, Laissue JA. Microbeam radiation therapy: clinical perspectives. Phys Medica 2015;31:564–7. https://doi.org/10.1016/j.ejmp.2015.02.011.
[2] Brauer-Krisch E, Serduc R, Siegbahn EA, Le Duc G, Prezado Y, Bravin A, et al. Effects of pulsed, spatially fractionated, microscopic synchrotron X-ray beams on normal and tumoral brain tissue. Mutat Res 2010;704:160–6. https://doi.org/10.1016/j.mrrev.2009.12.003.
[3] Livingstone J, Adam JF, Crosbie JC, Hall CJ, Lye JE, McKinlay J, et al. Preclinical radiotherapy at the Australian Synchrotron's Imaging and Medical Beamline: instrumentation, dosimetry and a small-animal feasibility study. J Synchrotron Radiat 2017;24:854–65. https://doi.org/10.1107/S1600577517006233.
[4] Smyth LM, Senthi S, Crosbie JC, Rogers PA. The normal tissue effects of microbeam radiotherapy: what do we know, and what do we need to know to plan a human clinical trial? Int J Radiat Biol 2016;92:302–11. https://doi.org/10.3109/09553002.2016.1154217.
[5] Laissue JA, Bartzsch S, Blattmann H, Brauer-Krisch E, Bravin A, Dallery D, et al. Response of the rat spinal cord to X-ray microbeams. Radiother Oncol 2013;106:106–11. https://doi.org/10.1016/j.radonc.2012.12.007.
[6] Mukumoto N, Nakayama M, Akasaka H, Shimizu Y, Osuga S, Miyawaki D, et al. Sparing of tissue by using micro-slit-beam radiation therapy reduces neurotoxicity compared with broad-beam radiation therapy. J Radiat Res 2017;58:17–23. https://doi.org/10.1093/jrr/rrw065.
[7] Slatkin DN, Spanne P, Dilmanian FA, Sandborg M. Microbeam radiation therapy. Med Phys 1992;19:1395–400. https://doi.org/10.1118/1.596771.
[8] Laissue JA, Blattmann H, Wagner HP, Grotzer MA, Slatkin DN. Prospects for microbeam radiation therapy of brain tumours in children to reduce neurological sequelae. Dev Med Child Neurol 2007;49:577–81. https://doi.org/10.1111/j.1469-8749.2007.00577.x.
[9] Slatkin DN, Spanne P, Dilmanian FA, Gebbers JO, Laissue JA. Subacute neuropathological effects of microplanar beams of x-rays from a synchrotron wiggler. Proc Natl Acad Sci USA 1995;92:8783–7. https://doi.org/10.1073/pnas.92.19.8783.
[10] Zhong N, Morris GM, Bacarian T, Rosen EM, Dilmanian FA. Response of rat skin to high-dose unidirectional x-ray microbeams: a histological study. Radiat Res 2003;160:133–42. https://doi.org/10.1667/3033.
[11] Laissue JA, Geiser G, Spanne PO, Dilmanian FA, Gebbers JO, Geiser M, et al. Neuropathology of ablation of rat gliosarcomas and contiguous brain tissues using a microplanar beam of synchrotron-wiggler-generated X rays. Int J Cancer 1998;78:654–60. https://doi.org/10.1002/(SICI)1097-0215(19981123)78:5<654::AID-IJC21>3.0.CO;2-L.
[12] Miura M, Blattmann H, Brauer-Krisch E, Bravin A, Hanson AL, Nawrocky MM, et al. Radiosurgical palliation of aggressive murine SCCVII squamous cell carcinomas using synchrotron-generated X-ray microbeams. Br J Radiol 2006;79:71–5. https://doi.org/10.1259/bjr/50464795.
[13] Siegbahn EA, Stepanek J, Brauer-Krisch E, Bravin A. Determination of dosimetrical quantities used in microbeam radiation therapy (MRT) with Monte Carlo simulations. Med Phys 2006;33:3248–59. https://doi.org/10.1118/1.2229422.
[14] De Felici M, Felici R, Sanchez del Rio M, Ferrero C, Bacarian T, Dilmanian FA. Dose distribution from x-ray microbeam arrays applied to radiation therapy: an EGS4 Monte Carlo study. Med Phys 2005;32:2455–63. https://doi.org/10.1118/1.1951043.
[15] Crosbie JC, Svalbe I, Midgley SM, Yagi N, Rogers PA, Lewis RA. A method of dosimetry for synchrotron microbeam radiation therapy using radiochromic films of different sensitivity. Phys Med Biol 2008;53:6861–77. https://doi.org/10.1088/0031-9155/53/23/014.
[16] Stepanek J, Blattmann H, Laissue JA, Lyubimova N, Di Michiel M, Slatkin DN. Physics study of microbeam radiation therapy with PSI-version of Monte Carlo code GEANT as a new computational tool. Med Phys 2000;27:1664–75. https://doi.org/10.1118/1.599034.
[17] Martinez-Rovira I, Sempau J, Prezado Y. Development and commissioning of a Monte Carlo photon beam model for the forthcoming clinical trials in microbeam radiation therapy. Med Phys 2012;39:119–31. https://doi.org/10.1118/1.3665768.
[18] Company FZ, Allen BJ. Calculation of microplanar beam dose profiles in a tissue/lung/tissue phantom. Phys Med Biol 1998;43:2491–501.
[19] Martinez-Rovira I, Sempau J, Fernandez-Varea JM, Bravin A, Prezado Y. Monte Carlo dosimetry for forthcoming clinical trials in x-ray microbeam radiation therapy. Phys Med Biol 2010;55:4375–88. https://doi.org/10.1088/0031-9155/55/15/012.
[20] Orion I, Rosenfeld AB, Dilmanian FA, Telang F, Ren B, Namito Y. Monte Carlo simulation of dose distributions from a synchrotron-produced microplanar beam array using the EGS4 code system. Phys Med Biol 2000;45:2497–508.
[21] Martinez-Rovira I, Sempau J, Prezado Y. Monte Carlo-based treatment planning system calculation engine for microbeam radiation therapy. Med Phys 2012;39:2829–38. https://doi.org/10.1118/1.4705351.
[22] Donzelli M, Brauer-Krisch E, Oelfke U, Wilkens JJ, Bartzsch S. Hybrid dose calculation: a dose calculation algorithm for microbeam radiation therapy. Phys Med Biol 2018;63:e045013https://doi.org/10.1088/1361-6560/aaa705.

[23] Schultke E, Balosso J, Breslin T, Cavaletti G, Djonov V, Esteve F, et al. Microbeam radiation therapy – grid therapy and beyond: a clinical perspective. Br J Radiol 2017;90:e20170073https://doi.org/10.1259/bjr.20170073.

[24] Bruzzaniti V, Abate A, Pedrini M, Benassi M, Strigari L. IsoBED: a tool for automatic calculation of biologically equivalent fractionation schedules in radiotherapy using IMRT with a simultaneous integrated boost (SIB) technique. J Exp Clin Cancer Res 2011;30:e52https://doi.org/10.1186/1756-9966-30-52.

[25] Grimm J, LaCouture T, Croce R, Yeo I, Zhu Y, Xue J. Dose tolerance limits and dose volume histogram evaluation for stereotactic body radiotherapy. J Appl Clin Med Phys 2011;12:267–92. https://doi.org/10.1120/jacmp.v12i2.3368.

[26] Mayo C, Yorke E, Merchant TE. Radiation associated brainstem injury. Int J Radiat Oncol Biol Phys 2010;76:S36–41. https://doi.org/10.1016/j.ijrobp.2009.08.078.

[27] Mayo C, Martel MK, Marks LB, Flickinger J, Nam J, Kirkpatrick J. Radiation dose–volume effects of optic nerves and chiasm. Int J Radiat Oncol Biol Phys 2010;76:S28–35. https://doi.org/10.1016/j.ijrobp.2009.07.1753.

[28] Kirkpatrick JP, van der Kogel AJ, Schultheiss TE. Radiation dose–volume effects in the spinal cord. Int J Radiat Oncol Biol Phys 2010;76:S42–9. https://doi.org/10.1016/j.ijrobp.2009.04.095.

[29] Marks LB, Bentzen SM, Deasy JO, Kong F-M, Bradley JD, Vogelius IS, et al. Radiation dose–volume effects in the lung. Int J Radiat Oncol Biol Phys 2010;76:S70–6. https://doi.org/10.1016/j.ijrobp.2009.06.091.

[30] Gagliardi G, Constine LS, Moiseenko V, Correa C, Pierce LJ, Allen AM, et al. Radiation dose–volume effects in the heart. Int J Radiat Oncol Biol Phys 2010;76:S77–85. https://doi.org/10.1016/j.ijrobp.2009.04.093.

[31] Pieters RS, Niemierko A, Fullerton BC, Munzenrider JE. Cauda equina tolerance to high-dose fractionated irradiation. Int J Radiat Oncol Biol Phys 2006;64:251–7. https://doi.org/10.1016/j.ijrobp.2005.04.019.

[32] Michalski JM, Gay H, Jackson A, Tucker SL, Deasy JO. Radiation dose–volume effects in radiation-induced rectal injury. Int J Radiat Oncol Biol Phys 2010;76:S123–9. https://doi.org/10.1016/j.ijrobp.2009.03.078.

[33] Lawrence YR, Li XA, el Naqa I, Hahn CA, Marks LB, Merchant TE, et al. Radiation dose–volume effects in the brain. Int J Radiat Oncol Biol Phys 2010;76:S20–7. https://doi.org/10.1016/j.ijrobp.2009.02.091.

[34] Serduc R, Bouchet A, Brauer-Krisch E, Laissue JA, Spiga J, Sarun S, et al. Synchrotron microbeam radiation therapy for rat brain tumor palliation-influence of the microbeam width at constant valley dose. Phys Med Biol 2009;54:6711–24. https://doi.org/10.1088/0031-9155/54/21/017.

[35] Regnard P, Le Duc G, Brauer-Krisch E, Tropres I, Siegbahn EA, Kusak A, et al. Irradiation of intracerebral 9L gliosarcoma by a single array of microplanar x-ray beams from a synchrotron: balance between curing and sparing. Phys Med Biol 2008;53:861–78. https://doi.org/10.1088/0031-9155/53/4/003.

[36] Schültke E, Bräuer-Krisch E, Blattmann H, Requardt H, Laissue JA, Hildebrandt G. Survival of rats bearing advanced intracerebral F 98 tumors after glutathione depletion and microbeam radiation therapy: conclusions from a pilot project. Radiat Oncol 2018;13:e89https://doi.org/10.1186/s13014-018-1038-6.

[37] Corbin KS, Hellman S, Weichselbaum RR. Extracranial oligometastases: a subset of metastases curable with stereotactic radiotherapy. J Clin Oncol 2013;31:1384–90. https://doi.org/10.1200/JCO.2012.45.9651.

[38] Lo SS, Moffatt-Bruce SD, Dawson LA, Schwarz RE, Teh BS, Mayr NA, et al. The role of local therapy in the management of lung and liver oligometastases. Nat Rev Clin Oncol 2011;8:e405https://doi.org/10.1038/nrclinonc.2011.75.

[39] Tree AC, Khoo VS, Eeles RA, Ahmed M, Dearnaley DP, Hawkins MA, et al. Stereotactic body radiotherapy for oligometastases. Lancet Oncol 2013;14:28–37. https://doi.org/10.1016/S1470-2045(12)70510-7.

[40] Hanif F, Muzaffar K. Perveen k, Malhi SM, Simjee SU. Glioblastoma multiforme: a review of its epidemiology and pathogenesis through clinical presentation and treatment. Asian Pac J Cancer Prev 2017;18:3–9.

[41] Young RM, Jamshidi A, Davis G, Sherman JH. Current trends in the surgical management and treatment of adult glioblastoma. Ann Transl Med 2015;3:e121https://doi.org/10.3978/j.issn.2305-5839.2015.05.10.

[42] Gallego O. Nonsurgical treatment of recurrent glioblastoma. Curr Oncol 2015;22:273–81. https://doi.org/10.3747/co.22.2436.

[43] Krathen RA, Orengo IF, Rosen T. Cutaneous metastasis: a meta-analysis of data. South Med J 2003;96:164–7. https://doi.org/10.1097/01.SMJ.0000053676.73249.E5.

[44] Balch CM, Buzaid AC, Soong S-J, Atkins MB, Cascinelli N, Coit DG, et al. Final version of the American Joint Committee on Cancer staging system for cutaneous melanoma. J Clin Oncol 2001;19:3635–48. https://doi.org/10.1200/JCO.2001.19.16.3635.

[45] Testori A, Faries MB, Thompson JF, Pennacchioli E, Deroose JP, van Geel A, et al. Local and intralesional therapy of in-transit melanoma metastases. J Surg Oncol 2011;104:391–6. https://doi.org/10.1002/jso.22029.

[46] Adams S, Kozhaya L, Martiniuk F, Meng T-C, Chiriboga L, Liebes L, et al. Topical TLR7 agonist imiquimod can induce immune-mediated rejection of skin metastases in patients with breast cancer. Clin Cancer Res 2012;18:6748–57. https://doi.org/10.1158/1078-0432.CCR-12-1149.

[47] Renier M, Brochard T, Nemoz C, Requardt H, Brauer E, Esteve F, et al. The radiotherapy clinical trials projects at the ESRF: technical aspects. Eur J Radiol 2008;68:S147–50. https://doi.org/10.1016/j.ejrad.2008.04.057.

[48] Emami B, Lyman J, Brown A, Coia L, Goitein M, Munzenrider JE, et al. Tolerance of normal tissue to therapeutic irradiation. Int J Radiat Oncol Biol Phys 1991;21:109–22. https://doi.org/10.1016/0360-3016(91)90171-Y.

[49] Hong AM, Millington S, Ahern V, McCowage G, Boyle R, Tattersall M, et al. Limb preservation surgery with extracorporeal irradiation in the management of malignant bone tumor: the oncological outcomes of 101 patients. Ann Oncol 2013;24:2676–80. https://doi.org/10.1093/annonc/mdt252.

[50] Hayashi K, Araki N, Koizumi M, Suzuki O, Seo Y, Naka N, et al. Long-term results of intraoperative extracorporeal irradiation of autogenous bone grafts on primary bone and soft tissue malignancies. Acta Oncol 2015;54:138–41. https://doi.org/10.3109/0284186X.2014.930172.

[51] Piazza M, Grady MS. Cranioplasty. Neurosurg Clin N Am 2017;28:257–65. https://doi.org/10.1016/j.nec.2016.11.008.

[52] Smyth LML, Donoghue JF, Ventura JA, Livingstone J, Bailey T, Day LRJ, et al. Comparative toxicity of synchrotron and conventional radiation therapy based on total and partial body irradiation in a murine model. Sci Rep 2018;8:e12044https://doi.org/10.1038/s41598-018-30543-1.

[53] Kirkpatrick JP, Meyer JJ, Marks LB. The linear-quadratic model is inappropriate to model high dose per fraction effects in radiosurgery. Sem Radiat Oncol 2008;18:240–3. https://doi.org/10.1016/j.semradonc.2008.04.005.

[54] Brenner DJ. The linear-quadratic model is an appropriate methodology for determining isoeffective doses at large doses per fraction. Sem Radiat Oncol 2008;18:234–9. https://doi.org/10.1016/j.semradonc.2008.04.004.

[55] van der Kogel AJ. Chronic effects of neutrons and charged particles on spinal cord, lung, and rectum. Radiat Res 1985;104:S208–16.

[56] Garcia LM, Leblanc J, Wilkins D, Raaphorst GP. Fitting the linear–quadratic model to detailed data sets for different dose ranges. Phys Med Biol 2006;51:2813. https://doi.org/10.1088/0031-9155/51/11/009.

[57] Marks LB, Yorke ED, Jackson A, Ten Haken RK, Constine LS, Eisbruch A, et al. Use of normal tissue complication probability models in the clinic. Int J Radiat Oncol Biol Phys 2010;76:S10–9. https://doi.org/10.1016/j.ijrobp.2009.07.1754.

[58] Ryu S, Pugh SL, Gerszten PC, Yin F-F, Timmerman RD, Hitchcock YJ, et al. RTOG 0631 phase II/III study of image-guided stereotactic radiosurgery for localized (1–3) spine metastases: phase II results. Pract Radiat Oncol 2014;4:76–81. https://doi.org/10.1016/j.prro.2013.05.001.

[59] Crosbie JC, Fournier P, Bartzsch S, Donzelli M, Cornelius I, Stevenson AW, et al. Energy spectra considerations for synchrotron radiotherapy trials on the ID17 biomedical beamline at the European Synchrotron Radiation Facility. J Synchrotron Radiat 2015;22:1035–41. https://doi.org/10.1107/S1600577515008115.

[60] Livingstone J, Stevenson AW, Hausermann D, Adam J. Experimental optimisation of the x-ray energy in microbeam radiation therapy. Phys Med 2018;45:156–61. https://doi.org/10.1016/j.ejmp.2017.12.017.

[61] Prezado Y, Fois G, Le Duc G, Bravin A. Gadolinium dose enhancement studies in microbeam radiation therapy. Med Phys 2009;36:3568–74. https://doi.org/10.1118/1.3166186.

[62] Shinohara K, Kondoh T, Nariyama N, Fujita H, Washio M, Aoki Y. Optimization of X-ray microplanar beam radiation therapy for deep-seated tumors by a simulation study. J Xray Sci Technol 2014;22:395–406. https://doi.org/10.3233/XST-140434.

[63] Lin H, Jing J, Xu L, Mao X. Monte Carlo study of the influence of energy spectra, mesh size, high Z element on dose and PVDR based on 1-D and 3-D heterogeneous mouse head phantom for Microbeam Radiation Therapy. Phys Med 2017;44:96–107. https://doi.org/10.1016/j.ejmp.2017.07.010.

[64] Livingstone J, Stevenson AW, Butler DJ, Häusermann D, Adam JF. Characterization of a synthetic single crystal diamond detector for dosimetry in spatially fractionated synchrotron x-ray fields. Med Phys 2016;43:4283–93. https://doi.org/10.1118/1.4953833.